Assessment of Mechanical Properties of Corroded Reinforcement in Chloride Environment Based on Corrosion Rate Monitoring

Grandić, Davor; Grandić, Ivana Štimac; Šćulac, Paulo

Source / Izvornik: **Civil Engineering Journal, 2024, 10, 3473 - 3492**

Journal article, Published version
Rad u časopisu, Objavljena verzija rada (izdavačev PDF)

https://doi.org/10.28991/CEJ-2024-010-11-02

Permanent link / Trajna poveznica: https://urn.nsk.hr/urn:nbn:hr:157:552215

Available online at www.CivileJournal.org

Civil Engineering Journal

(E-ISSN: 2476-3055; ISSN: 2676-6957)

Vol. 10, No. 11, November, 2024

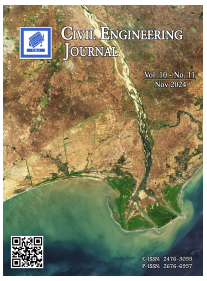

Assessment of Mechanical Properties of Corroded Reinforcement in Chloride Environment Based on Corrosion Rate Monitoring

Davor Grandić [1*], Ivana Štimac Grandić [1], Paulo Šćulac [1]

[1] *Faculty of Civil Engineering, University of Rijeka, Radmile Matejčić 3, 51000 Rijeka, Croatia.*

Received 19 August 2024; Revised 16 October 2024; Accepted 23 October 2024; Published 01 November 2024

Abstract

Existing models for the evaluation of mechanical properties of corroded reinforcement, defined as a function of the mean cross-sectional loss or mass loss of the reinforcement, are not suitable in the case of chloride-induced corrosion, which causes irregular corrosion attack with pronounced localized damage—pits, whose geometry and spacing have a major influence on the mechanical properties of the reinforcement. Models that consider the irregularity of damage due to chloride corrosion are efficient, but as with models based on cross-sectional or mass loss, it is necessary to extract corroded rebars from the reinforced-concrete structure, which is a destructive procedure that can only be performed to a limited extent on an in-service building. To fill the above gaps, a new method based on the non-destructive measurement of corrosion parameters is proposed. The corrosion depth determined from the monitoring correlates directly with the remaining mechanical properties of the reinforcement; therefore, it is not necessary to determine the remaining cross-sectional area and geometry of the pits. The proposed models are based on experimental research on reinforced-concrete beam specimens subjected simultaneously to sustained loading and accelerated chloride corrosion in an environmental chamber in order to induce corrosion similar to that on real structures.

Keywords: Pitting Corrosion; Corrosion Rate Monitoring; Mechanical Properties; Corroded Reinforcement; Accelerated Corrosion.

1. Introduction

The proportion of reinforced concrete (RC) in building construction stock is around 50% and sometimes even higher in infrastructure projects such as dams, marine structures, etc. [1]. Although RC structures have many advantages (e.g., cost efficiency, ease of modelling into any desired shape, high compressive strength, durability, etc.), they are subject to deterioration when exposed to harsh environmental conditions over the long term, resulting in a significant number of RC structures not reaching their intended service life and causing significant economic losses [2–4]. According to Bras et al. [5], the cost of maintaining and repairing existing structures in the UK, most of which are RC structures, is around £40 billion a year. The most common cause of premature deterioration of RC structures is corrosion of reinforcement, especially for those structures exposed to de-icing salts or in a marine environment [3, 5–7]. High-income countries spend up to 3 to 5% of the gross domestic product (GDP) to mitigate the effects of reinforcement corrosion [8]. Similar data is available for India, where RC corrosion costs are between 3–4% of annual GDP [5]. In the UK, £23 billion a year is spent on corrosion-damaged RC structures [5].

In many cases, extensive and expensive repairs could be avoided through appropriate inspection, monitoring, and maintenance measures. It is therefore extremely important to have a reliable tool to assess the condition of RC structures exposed to reinforcement corrosion (the remaining load-bearing capacity, serviceability, and ductility), which forms the

* Corresponding author: davor.grandic@gradri.uniri.hr

http://dx.doi.org/10.28991/CEJ-2024-010-11-02

basis for decisions on the management of structural maintenance and repair. The mechanical properties of the reinforcement are very important for assessing the actual condition of the RC members in order to determine their resistance and load-bearing capacity [9].

Reinforcing steel in RC structures does not corrode under normal conditions, as there is a protective layer around the reinforcing bars. The destruction of the protective layer is caused by the action of carbonation or chlorides on the RC [10]. Carbonation of the concrete leads to homogeneous corrosion, while the presence of chlorides in concrete results in localized (pitting) corrosion [11]. The corrosion attack not only reduces the reinforcement cross-sectional area but also alters the constitutive law of the reinforcement [12], resulting in a deterioration of the strength and ductility of the reinforcing bars [13–17]. In both cases (carbonation and chloride phenomena), the mechanical properties of the steel bars decrease, while pitting corrosion causes a greater reduction in the mechanical properties [12, 17].

Although the issue of degradation of RC structures subject to corrosion has attracted much attention over the last four decades, the effects of corrosion on the mechanical properties of reinforcing steel are still being investigated. Since natural corrosion is a long-term process, most researchers resort to accelerating corrosion using the impressed current technique [18], while others create an artificial climate environment to accelerate corrosion by simulating the natural conditions, such as [7, 9, 19–23]. Some of them combine the impressed current and artificial climate environment, e.g., [24, 25]. Only a few research papers contain results on the mechanical properties of corroded reinforcement after long-term tests on RC members exposed to natural corrosion [18, 26–31].

In some studies, bare reinforcement bars are subjected to accelerated corrosion under impressed current [9, 16, 17, 19, 23]. Apart from the fact that the tests with bare reinforcement bars are questionable because the experimental setup does not simulate the actual conditions under which the bar is embedded in the RC structure, it has also been shown that it is not easy to simulate pitting corrosion on the bare bars experimentally (the corrosion is almost uniform) [9, 17].

A better simulation of the natural state is achieved by embedding the steel reinforcement into the concrete. Specimens of different shapes and sizes [7, 16, 17, 19–21, 26, 32, 33] were prepared and tested under different corrosion conditions in order to determine the remaining mechanical properties of the reinforcement. Although Imperatore et al. [17] state that steel bars embedded into a concrete prism exhibit locally pronounced pits when artificially corroded under anodic current, it should be noted that many researchers detected that the common technique of corrosion acceleration by impressed current leads to uniform corrosion, which is not representative of natural chloride-induced corrosion [18, 19, 34–36].

To induce chloride corrosion similar to that on real structures, it is therefore necessary to reproduce environmental conditions that are similar to those in nature. Real environmental conditions are usually simulated by creating an artificial climate environment in a chamber (environmental/climate chamber) [7, 9, 19–22]. Yuan et al. [19] showed that the process and corrosion characteristics of the steel bars under artificial climate environments are similar to those of chloride corrosion under natural environments.

Apart from the fact that RC specimens should be exposed to real environmental conditions (temperature, humidity, and chlorides), concrete cracks regularly occur under service load, i.e., during regular use of the RC structures. Numerous studies were conducted on the effects of the cracks on the distribution of chloride-induced reinforcement corrosion, and it has been demonstrated that the corrosion rate of the pit increases in the vicinity of a crack [36]. It is therefore important that the specimens have cracks (caused by bending or tensile force) before they are exposed to chloride corrosion in the environmental chamber. Unfortunately, there are not many studies on the deterioration of the mechanical properties of corroded reinforcement performed under environmental conditions (either in real time or accelerated) on cracked specimens. The most extensive studies on naturally induced chloride corrosion on specimens under sustained loading have been carried out by a research group from the University of Toulouse [7, 27–30].

Over the years, many constitutive models for the decay of the mechanical properties of corroded reinforcement have been established, but they differ considerably, as most experimental programs were carried out under different conditions [18]. Despite all the differences, there is a general agreement on the reduction of the constitutive law determined on the initial cross section of uncorroded reinforcement when the steel reinforcement corrodes [12]. Furthermore, the observed decrease in ductility was significantly greater than the decrease in tensile strength [12, 13].

Most models for the degradation of the mechanical properties of reinforcement due to corrosion are based on the reduction of the cross-sectional area or mass of the reinforcement [12, 18]. In many cases, the cross-sectional loss is calculated based on the mass loss of the rebar, which only gives the average cross-sectional loss over the rebar length. The assessment of the loss of mechanical properties based on the mass loss or the average cross-sectional loss is more suitable for corrosion caused by carbonation (homogeneous corrosion), where the cross-sectional loss does not change much along the rebar [12]. In the case of pitting corrosion, where inhomogeneous corrosion is observed both across the cross-section and along the rebar, the models based on mass loss are not suitable [12], which is why different models based on the remaining cross-sectional area have been developed.

Models presented in Rodríguez et al. [37, 38], which relate the remaining mechanical properties only to the residual cross-sectional area, give the estimation of the residual cross-sectional area as a function of the remaining diameter of the corroded reinforcement ϕ according to Figure 1. a) and b) (area denoted as grey circle in the cross-section). In Figure 1, ϕ_0 denotes the initial bar diameter of uncorroded bar, $P_{i,\text{corr}}$ is the mean corrosion depth, P_{pit} is the pit depth, while α represents the pitting factor.

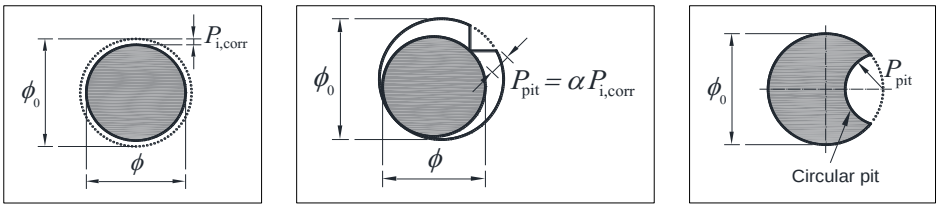

a) b) c)

Figure 1. Residual cross-section of corroded reinforcing bars: a) homogenous corrosion (adapted from Rodríguez et al. [37, 38]), b) pitting corrosion (adapted from Rodríguez et al. [37, 38]), c) pitting corrosion (adapted from [13, 39–41])

The pit depth P_{pit} can be determined only by measurement on the corroded reinforcing bar, while the mean corrosion depth $P_{i,\text{corr}}$ can be determined from the difference between the uncorroded and the corroded bar masses [42] or from the corrosion rate measurements results collected during the monitoring of RC structures using non-destructive electrochemical methods [37, 38, 43, 44]. The value of the pitting factor α depends on the reinforcement corrosion type. If the reinforcement is subjected to homogeneous corrosion, the pitting factor α is equal to 2 (Figure 1-a), while in the case of pitting corrosion, the factor α depends on the corrosion progression: the highest α are for lower corrosion levels (the pitting factor α obtained using the linear polarization method can be up to 10 [37, 38, 42]), and as corrosion progresses, the α values decrease [7, 45].

In the case of pitting corrosion, the residual cross-section of the corroded reinforcement determined according to the model presented in Rodríguez et al. [37, 38] is a rather conservative value, as can be seen in Figure 1-b. A less conservative model for estimation of the residual cross-sectional area of the corroded reinforcing bars caused by pitting corrosion is presented in [13, 39–41], where a circular shape of the pit is assumed (Figure 1-c). Still, with this simplified idealization of the residual cross-sectional area of the corroded reinforcing bars, it is not possible to cover all cases of pitting corrosion, since the pitting corrosion can cause pits with different shapes, lengths, and depths [27, 32, 46–49].

The residual cross-sectional area of corroded reinforcing bars as well as the shape and distribution of corrosion damage along the bars can be determined using laser and optical 3D scanning methods [32, 47–50]. Since these are light-based methods, they can only detect corrosion damage that can be penetrated by light. If the pits are irregularly shaped or expand in depth, they may not be fully detected. In addition, the accuracy of the 3D scanner can be a limiting factor for these methods. Experiments have shown that first cracks in concrete appear at an average corrosion penetration of 50 μm in the reinforcement [38]. X-ray tomography can also be used to determine localized corrosion damage to reinforcing bars [51].

Regardless of the accuracy of the technique used to determine the residual cross-sectional area of the corroded reinforcement, it should also be taken into account that the cross-section loss is not the only factor affecting the mechanical properties of the corroded reinforcement. The shape and arrangement of the localized corrosion (pits) also have a significant influence on the mechanical properties of the corroded reinforcement [27, 49, 52]. A similar conclusion was drawn in Imperatore [12] and Ou et al. [53]. Due to the different shapes and the non-uniform arrangement of the pits along the rebar, it is quite difficult to establish a relationship between the mechanical properties of the corroded reinforcement and the shape of the pits. Therefore, several studies have been carried out on bars in which pits of a certain shape were machine-made [13, 27, 52, 54], while some authors have used numerical simulations to evaluate the influence of the pit shape and pit distribution on the mechanical properties of corroded reinforcement [13, 55]. Studies on machine-made pits showed that different corrosion morphologies lead to significantly different degradation rates with the degree of corrosion. Hingorani et al. [55] conducted a detailed numerical study of pitting corrosion using the finite element method in which they modelled the bar with a pit in the form of an ellipsoid with radii a (pit length in the direction of the bar axis), b (pit width in the direction perpendicular to the bar axis) and P_{pit} (pit depth measured from the original surface of the bar). The ratio a/P_{pit} was varied in the study, while the pit width was constant $b=P_{\text{pit}}$.

The following conclusions were drawn: (i) the yield strength and the tensile strength, which were determined in relation to the initial cross-sectional area of the uncorroded bars, decrease significantly with increase of the relative pit depth P_{pit}/ϕ_0, (ii) the ductility of the bars decreases significantly with increase of the relative pit depth P_{pit}/ϕ_0, (iii) at a constant relative pit depth P_{pit}/ϕ_0, the ductility of the bars increases with the increase in the pit length to pit depth ratio a/P_{pit}, (iv) the relationship between the increase of the relative pit depth and the reduction in the yield strength is not linear, i.e. the gradient of the reduction of the yield strength increases with the increase of the pit depth, (v) the variation

of the tensile strength to yield strength ratio ($k = f_t/f_y$) for bars with pits to the corresponding strength ratio of initial bar ($k_0 = 1.08$) is neglectable up to relative pit depths $P_{pit}/\phi_0 = 0.2$, (vi) the strain at tensile strength ε_u decreases rapidly up to the relative pit depth $P_{pit}/\phi_0 \approx 0.1$. An important conclusion of the study Hingorani et al. [55] is that there is no scale effect - the bar diameter has no influence on the mechanical properties of the reinforcement if the mechanical properties are determined as a function of the relative pit depth P_{pit}/ϕ_0.

As already mentioned, the 3D laser scanning method is nowadays used to investigate the shape of corroded reinforcement [47–50]. In Chen et al. [49] the combination of 3D scanning and digital image correlation (DIC) was used to describe the mechanical behavior of reinforcing bars with pitting corrosion. The bars were extracted from RC beams that were first subjected to loading in a three-point bending configuration, what caused cracks, and then exposed to cyclic wet-dry exposure to a chloride solution, which is an accelerated simulation of the natural corrosion process, as opposed to corrosion by a direct current source [19]. In this way, localized reinforcement corrosion was induced, which is very similar to natural conditions [19]. The non-homogeneous distribution of the residual cross-sectional area of the reinforcing bars with localized pitting corrosion was determined by 3D scanning. After 3D scanning, tensile tests were performed on the corroded bars. In the tensile tests, the strains on the bars were measured using the DIC technique. The DIC technique showed a non-uniform distribution of strains along the bars – i.e. the strains were significantly larger at the pit locations. It was shown that the ductility of the reinforcement decreases significantly with increasing degree of localized corrosion (at the pit locations). Based on the research results, they proposed an analytical and a semi-analytical model for estimation of the limit strains of corroded reinforcement. They also pointed out that a longer bar length should be taken into account, i.e. only results obtained with strain gauges longer than 10 cm are reliable.

The presented models for evaluation of the mechanical properties of reinforcement subjected to pitting corrosion are performed by measuring and observing corrosion damage on rebars and relating this damage to the remaining mechanical properties of the corroded bars. Most of the models are related to the mass loss or cross-sectional loss. As already mentioned, models based on the mass loss have potential for carbonate corrosion; they are not suitable for chloride corrosion. Models based only on the cross-sectional loss do not take into account the shape and distribution of pits along the bar, which have been shown to be a relevant parameter for the mechanical properties of the reinforcement (especially ductility). In our opinion, the methods and models proposed in [49] to evaluate the mechanical properties of corroded reinforcement, which take into account the shape and distribution of corrosion damage on the bars, are very efficient. However, the disadvantage of this approach is that it is not possible to extract corroded rebars from RC structures that are still in-service in order to perform a detailed 3D scanning.

To overcome the above shortcomings, this paper proposes practical models to evaluate the mechanical properties of corroded reinforcement required for the condition assessment of corroded RC structures using non-destructive measurements. According to Shevtsov et al. [3], the most common non-destructive monitoring methods used to determine the corrosion condition are electrochemical methods, such as the galvanostatic pulse technique (GPT), linear polarization resistance (LPR), half-cell potential (HCP) and electrochemical impedance spectroscopy (EIS). The GPT used in this research is a fast and cost-effective technique that provides more stable and accurate results than LPR measurements under adverse conditions [3]. It is also more stable and accurate than HCP, LPR and EIS when a stable reference electrode is not available [3].

The proposed models for determining the yield strength, tensile strength, tensile strength to yield strength ratio, modulus of elasticity and strain at maximum load are based on the results of an extensive long-term experimental study on RC beams subjected to simultaneous loading and accelerated chloride corrosion in an environmental chamber. The evaluation of models based on non-destructive GPT measurements was carried out by creating comparative models based on the destructive method and by comparison with literature data.

1.1. Research Significance

The degradation models of the mechanical properties of hot rolled steel reinforcement are established based on results obtained in experimental research on RC beams subjected to sustained load and accelerated chloride corrosion in an environmental chamber. This is the best way to simulate the corrosion effects that occur on real RC structures.

All mechanical properties of the corroded reinforcement are determined in relation to the initial cross-sectional area of uncorroded reinforcement, while the corrosion progress is defined in relation to the initial diameter of the uncorroded reinforcement. The degradation models are expressed in relation to the mechanical properties of uncorroded reinforcement and corrosion progress; only the corrosion rate measurements using non-destructive monitoring technique on the RC structure are required to determine the remaining mechanical properties of the corroded reinforcement.

The proposed method for evaluation of the mechanical properties of corroded reinforcement via corrosion monitoring using the galvanostatic pulse technique therefore offers great potential for assessing the remaining load-bearing capacity, serviceability and ductility of RC structures exposed to reinforcement corrosion in a chloride environment. Figure 2 illustrates the flowchart showing the process of the research methodology.

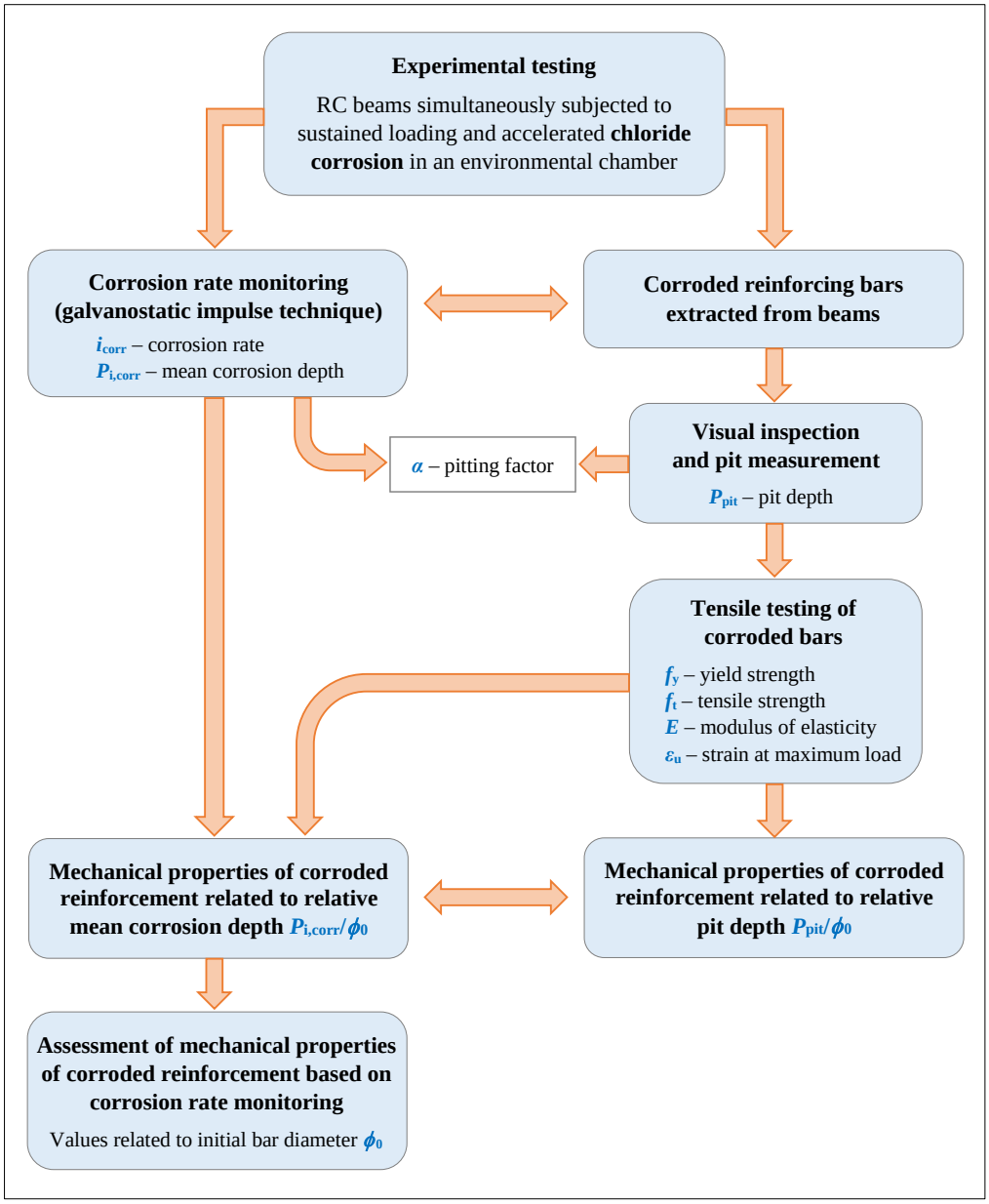

Figure 2. Flowchart of the research methodology

2. Experimental Programme

An extensive experimental research was carried out in which a series of 12 RC beam specimens (shorter: beam specimens) were simultaneously subjected to sustained loading and accelerated chloride corrosion in an environmental chamber for a total of 383 days. The experimental setup is presented in detail in [56]. The initiation of reinforcement corrosion in the beam specimens and its acceleration was performed by repeating the cycles of wetting and drying [20, 21, 45]. Each cycle lasted three days. On the first day, specimens were sprayed with salt water. The salinity of water of 38 %. (NaCl concentration) was selected to correspond to the salinity of the Adriatic Sea. On the second day, the specimens were exposed to an air temperature of about 20°C and a relative humidity of about 70%. On the third day, the environmental chamber was heated for 3 hours up to a temperature of 50°C or slightly higher, with simultaneous ventilation with fans, so that the relative humidity dropped to 20%. One day in each week (Sunday) was a day without spraying or heating. A total of 109 cycles were performed.

The beam specimens were 200 cm long and had a cross-section of 8×12 cm (Figure 3). The concrete cover was 1.0 cm. The beams were reinforced with deformed bars: 2 bars of 8 mm nominal diameter in the bottom zone and 2 bars of 6 mm nominal diameter in the upper zone, while the stirrups with nominal diameter of 6 mm were distributed over the beam at a distance of 8 cm. The 8 mm bars were made of hot-rolled reinforcing steel, while the 6 mm bars were made of cold-worked reinforcing steel. The material properties of the beam specimens determined by laboratory tests can be found in [20, 45]: the results indicate that the beam specimens were made of medium-quality concrete regarding transport-related properties [57, 58].

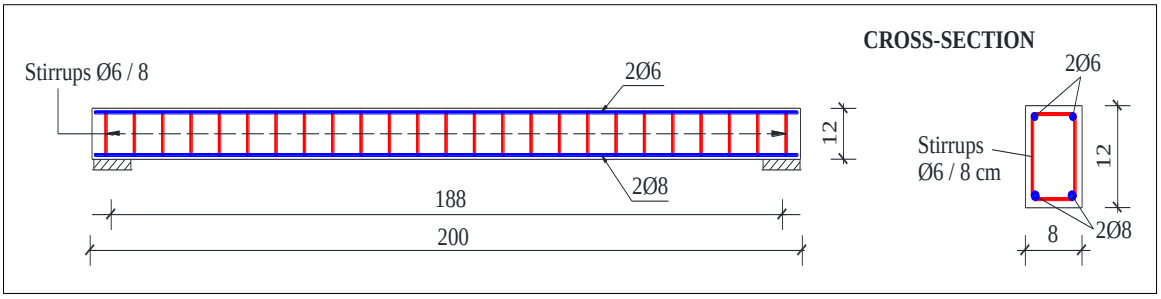

Figure 3. Geometry and reinforcement layout of beam specimens (dimensions in cm)

During accelerated chloride corrosion, the beam specimens were subjected to constant sustained loading (four-point bending configuration) in steel loading frames (Figures 4 and 5) in order to produce cracks in beam specimens with an average width of 0.1 mm (Figure 6). According to Li et al. [59, 60], a crack that is 0.1 mm wide or more significantly increases the penetration of chlorides, depassivation, and the occurrence of reinforcement corrosion, regardless of the thickness of the concrete cover and the concrete quality.

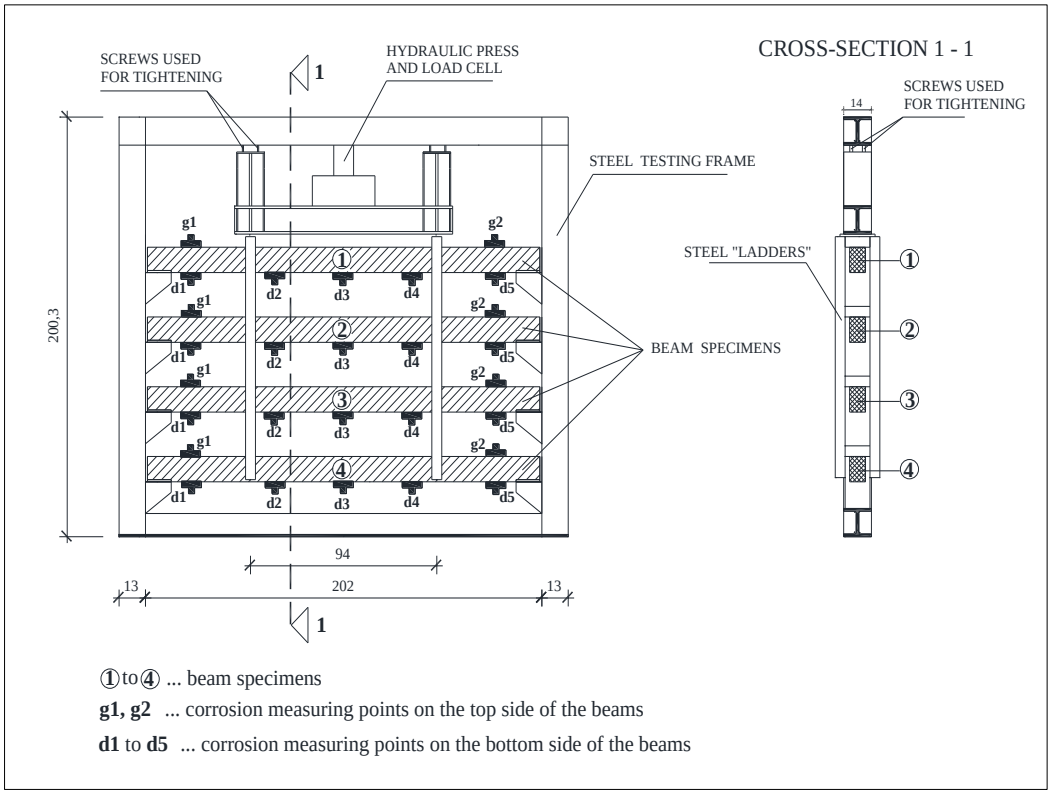

Figure 4. Experimental setup: four-point bending loading frame with beam specimens (dimensions in cm)

Figure 5. Beam specimens in the loading frame

Figure 6. Cracks caused by sustained loading

The loading frame with beam specimens and the corrosion measuring points are shown in Figure 4. The beam specimens were labelled as GI-1 to GI-4, GII-1 to GII-4 and GIII-1 to GIII-4, where I, II or III denotes series of beam specimens where different corrosion levels were achieved (corrosion levels I, II or III respectively), while labels 1 to 4 indicate the position of the beam specimen in the loading frame (1 – at the top, 4 – at the bottom of the frame).

The experimental programme comprised of three corrosion levels. Corrosion level I corresponded to the value of the mean corrosion depth equal to $P_{i,corr} \approx 0.05$ mm, corrosion level II corresponded to 0.1 mm $\leq P_{i,corr} \leq 0.2$ mm, while $P_{i,corr} > 0.2$ mm refers to the corrosion level III. The achieved values of the mean corrosion depth $P_{i,corr}$ were determined using the electrochemical galvanostatic pulse technique. A series of four beam specimens were used for each corrosion level.

Data have been collected on the progression of chloride corrosion and the damaging effects of corrosion on RC beam specimens [20, 21, 45]. The corrosion parameters such as the corrosion rate, half-cell potential and electrical resistance were measured at regular intervals on beam specimens. After reaching each of the three corrosion levels, one beam specimen from the corresponding specimen series was removed from the loading frame. The reinforcing bars were then extracted from these beam specimens to perform a detailed visual inspection, length and mass measurement and tensile testing.

3. Experimental Results

Within the experimental research, the corrosion parameters were measured in 18 phases with GalvaPulse^{TM}. The GalvaPulse^{TM} device, based on the galvanostatic impulse technique [20, 21], measures the corrosion rates (corrosion current density i_{corr}) in relation to the surface area of the bar within the specified measuring range of the sensor [44, 61]. The standard diameter of the measuring range of the sensor (GalvaPulse^{TM}) of 70 mm was used [62]. The corrosion parameters were measured at two points on the top side (g1 and g2) and at five points on the bottom side (d1 to d5) on each beam specimen. Detailed data on the measured corrosion parameters can be found in [20].

Five reinforcing bar specimens (shorter: bar specimens) were extracted from the bottom longitudinal reinforcement of each beam specimen removed from the loading frame after particular corrosion level has been reached. The bar specimens were labelled 1 to 5, where numbers 1 to 5 denote to the location of the corrosion measurement points on the bottom side of the beams d1 to d5 (Figure 4).

3.1. Corrosion Parameters

The mass loss and the depth of corrosion penetration were determined on each bar specimen. The mass loss was determined by weighting each corroded bar specimen and subtracting it from the initial mass of the uncorroded reinforcement. Detailed information on determination of mass loss is presented in [45]. The initial length mass m_0 determined by weighting of the uncorroded reinforcement for a nominal bar diameter of 8 mm was 0.4264 g/mm. The diameter of an ideally round cross-section of uncorroded reinforcement (i.e. initial bar diameter ϕ_0) can be determined at a steel density of 0.00785 g/mm^3 as $\phi_0 = 12.74 \cdot \sqrt{m_0} = 8.3193$ mm, while the mean value of the initial cross-sectional area of the bar (determined for ϕ_0) is $A_0 = 54.4$ mm^2.

The pit depths P_{pit} presented in Table 1 were measured with a point micrometer at the location of the deepest pit on the corroded bar specimens [45]. The mean corrosion depth $P_{i,corr}$ in μm in the measuring range of the sensor may be obtained from the corrosion rates according to Poulsen [44] using the following expression [20, 21, 45]:

$$P_{i,corr} = 11.6 \cdot \int_{t0}^{\tau} i_{corr} dt \quad (1)$$

where i_{corr} is the corrosion rate at time t in μA/cm^2, (τ - t_0) indicates the duration of corrosion in years, t_0 is the time when corrosion was initiated and τ is the time at which $P_{i,corr}$ is calculated. The constant value of 11.6 is the conversion factor for corrosion rate in μA/cm^2 to the corrosion rate in μm/year, obtained using Faraday's law [37, 38]. The mean corrosion depths $P_{i,corr}$, shown in Table 1, were determined according to Equation 1 from the corrosion rate measurements at points d1 to d5 [20, 45].

Table 1. Values determined on corroded bar specimens [45]

Corrosion level, beam specimen	Bar specimen	P_{pit} [mm]	$P_{i,corr}$ [mm]	α	P_{pit}/ϕ_0	$P_{i,corr}/\phi_0$	Mass loss [%]
Corrosion level I, beam GI-4	1	0.31	0.037	8.53	0.037	0.004	3.80
	2	0.28	0.065	4.35	0.034	0.008	3.96
	3	0.30	0.055	5.48	0.036	0.007	3.52
	4	0.24	0.055	4.41	0.029	0.007	3.92
	5	0.22	0.044	5.10	0.026	0.005	4.10
Corrosion level II, beam GII-3	1	0.35	0.113	3.12	0.042	0.014	7.60
	2	0.37	0.155	2.41	0.044	0.019	7.65
	3	0.37	0.197	1.90	0.044	0.024	7.75
	4	0.33	0.205	1.62	0.040	0.025	7.66
	5	0.34	0.112	3.08	0.041	0.013	7.33
Corrosion level III, beam GIII-4	1	0.50	0.147	3.42	0.060	0.018	7.17
	2	0.67	0.246	2.74	0.081	0.030	7.70
	3	0.61	0.245	2.50	0.073	0.029	7.93
	4	0.59	0.289	2.05	0.071	0.035	7.72
	5	0.44	0.159	2.79	0.053	0.019	7.33

The correlation between the maximum corrosion depth (i.e. the pit depth P_{pit}) and the mean corrosion depth $P_{i,corr}$ in case of localized corrosion is defined by the pitting factor α [40]:

$$\alpha = \frac{P_{pit}}{P_{i,corr}} \quad (2)$$

The values of the pitting factor α, obtained from experimentally determined values P_{pit} and $P_{i,corr}$ are presented in Table 1. The relative corrosion depths P_{pit}/ϕ_0 and $P_{i,corr}/\phi_0$, related to the initial bar diameter ϕ_0 are also shown in Table 1, as well as mass losses. A strong correlation between the relative mean corrosion depths $P_{i,corr}/\phi_0$, which were determined from the corrosion rate measurement results, and the pitting factor α was established (Figure 7).

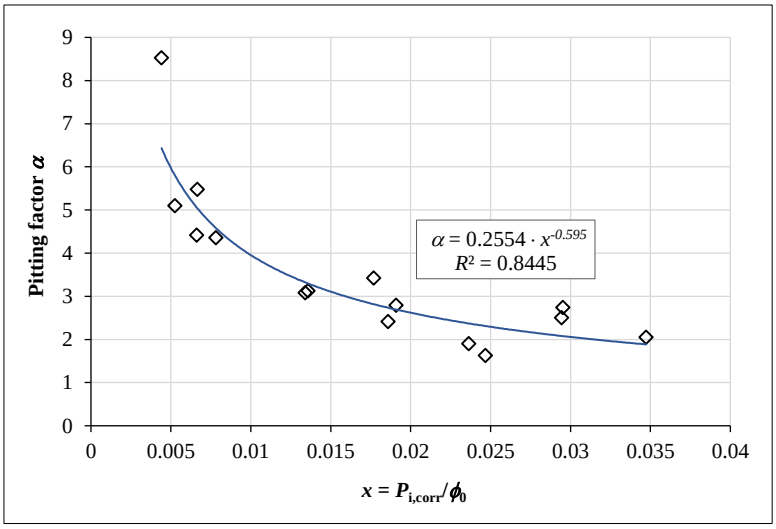

Figure 7. Relation between the pitting factor α and the relative mean corrosion depth $P_{i,corr}/\phi_0$

It can be observed that the highest pitting factor α equal to 8.53 corresponds to the corrosion level I (Table 1). As the reinforcement corrosion advances, the pitting factor α rapidly decreases and equals approximately to 2.0 at relative mean corrosion depth $P_{i,corr}/\phi_0$ greater than 0.03 (Table 1 and Figure 7). The decrease of the pitting factor α with increase of the reinforcement corrosion is also shown in Yu et al. [7] and Cairns et al. [13]. The pitting factor in [7] was determined as the ratio of the local and the average loss of the bar cross-section, while in Cairns et al. [13] it is determined as a ratio between the maximum and the average corrosion penetration. The progression of reinforcement corrosion was described as an increase in the mean cross-sectional loss [7]. The trends of the change of the pitting factor in Yu et al. [7] and Cairns et al. [13] are similar as shown in Figure 7: for small values of section loss, the pitting factor α has the highest values but decreases rapidly with the increase of section loss. For significant section losses (more than 5%), the downward trend of the pitting factor α slows down considerably [7].

3.2. Mechanical Properties of the Reinforcing Bars

Due to cracks in concrete, the reinforcing bars in the region of the maximum bending moment are significantly more corroded, and their condition has a significant impact on the behavior of the beam under loading (load-bearing capacity, deflection and cracks). The corrosion progress of the reinforcement was 1.6 times higher in terms of corrosion penetration depth in the region of the maximum bending moment than in the remaining part of the beam [20]. Therefore, the mechanical properties of corroded reinforcing bars were determined on bar specimens labeled 2 to 4 (Table 1) of bottom longitudinal reinforcement extracted from the middle part of the beam span (region with constant bending moment, between two concentrated forces – corrosion measuring points d2 to d4: see Figure 4). The mechanical properties of uncorroded bars were also determined.

The bar specimens were loaded in tension; stress-strain diagrams were obtained until failure. The tests were carried out in accordance with the EN standard [63] using the Zwick Z600E universal testing machine and TestExpert software. During the tests, force and elongation were measured within the 150 mm extensometer gauge length. The extensometer gauge length was selected to take into account the influence of localized corrosion on the average strain of the tensile bars, which is necessary for assessing the behavior of RC members with corroded reinforcement under loading [49].

The stress-strain diagrams and the mechanical properties of three uncorroded bar specimens labeled 1 to 3 are shown in Figure 8 and Table 2. The mechanical properties and stress-strain diagrams of corroded bars were determined in relation to the mean value of the initial cross-sectional area of the uncorroded bar A_0 and are shown in Figures 9 to 11 and Table 2.

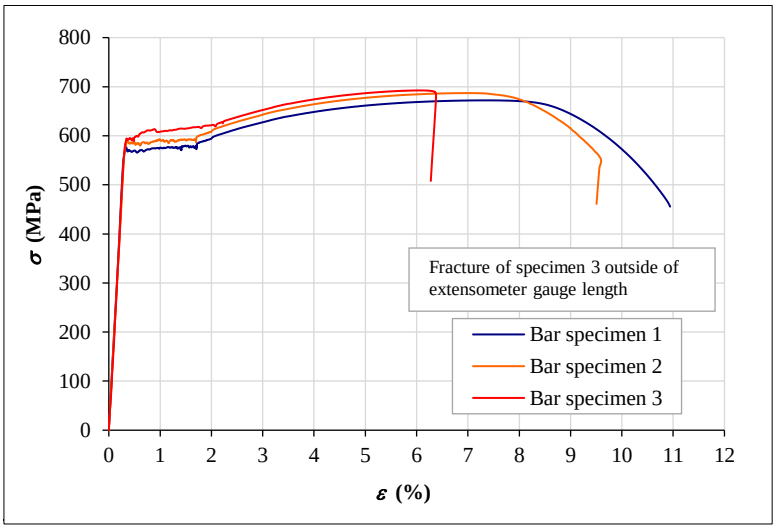

Figure 8. Stress-strain diagrams of uncorroded bars

Table 2. Mechanical properties of uncorroded and corroded bars with nominal diameter of 8 mm

Corrosion level, beam specimen	Bar specimen	Modulus of elasticity E (MPa)	Yield strength f_y (MPa)	Tensile strength f_t (MPa)	Ratio of tensile strength to yield strength $k = f_t/f_y$	Strain at maximum load ε_u (%)
Uncorroded	1	191750	581	672	1.16	7.42
	2	184900	592	687	1.16	7.11
	3	198770	593	692	1.17	6.25
	Mean value	191807	589	684	1.16	6.93
Corrosion level I, beam GI-4	2	160100	556	653	1.17	6.94
	3	183630	533	657	1.23	5.53
	4	174340	544	626	1.15	4.19
	Mean value	172690	544	645	1.18	5.55
Corrosion level II, beam GII-3	2	153090	511	625	1.22	5.24
	3	184090	525	624	1.19	5.71
	4	176550	540	639	1.18	6.07
	Mean value	171243	525	629	1.20	5.67
Corrosion level III, beam GIII-4	2	175170	503	605	1.20	4.09
	3	189240	520	630	1.21	6.91
	4	168360	511	596	1.17	3.76
	Mean value	177590	511	610	1.19	4.92

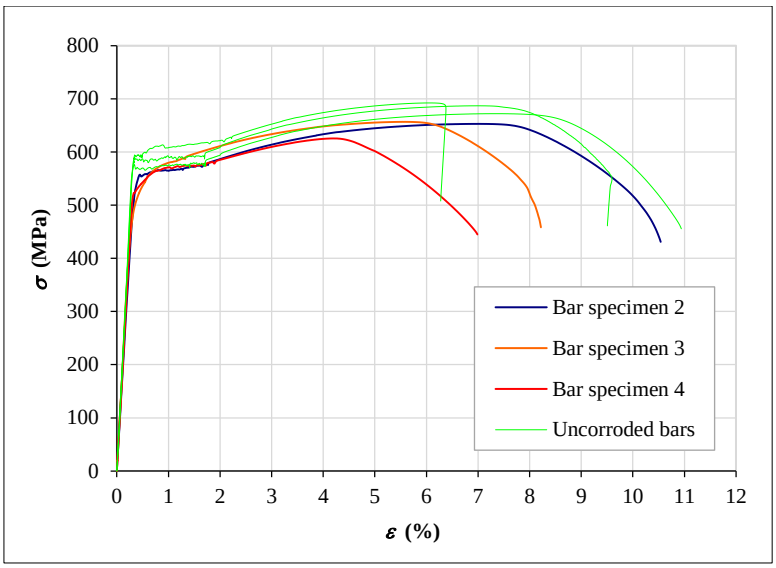

Figure 9. Stress-strain diagrams of corroded bars extracted from beam specimen GI-4, corrosion level I

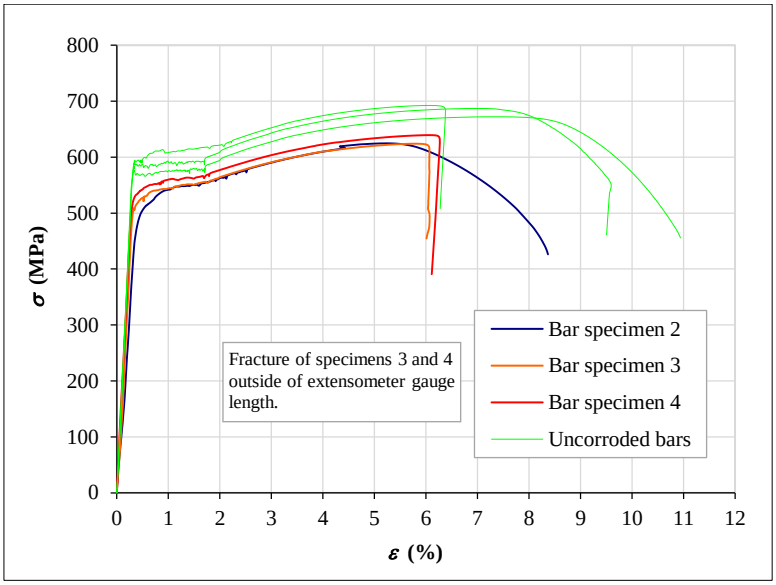

Figure 10. Stress-strain diagrams of corroded bars extracted from beam specimen GII-3, corrosion level II

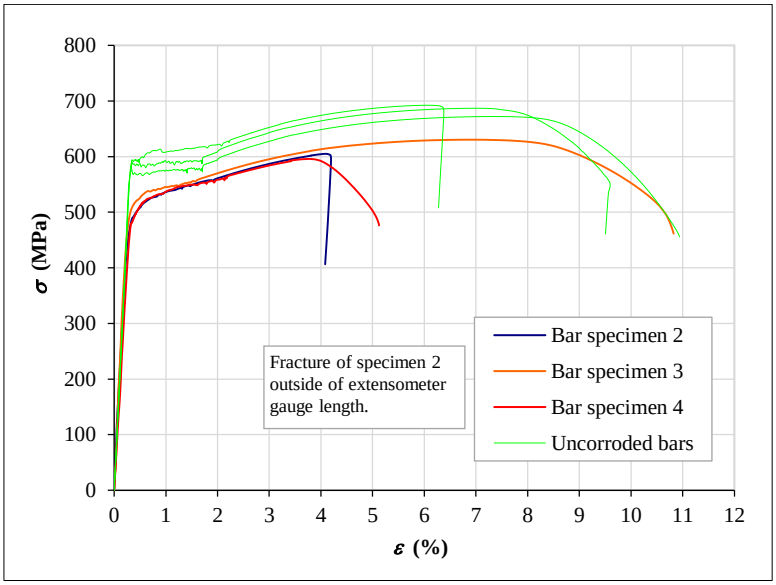

Figure 11. Stress-strain diagrams of corroded bars extracted from beam specimen GIII-4, corrosion level III

The stress-strain diagrams of corroded bars (Figures 9 to 11) show a similar general behavior as observed in previous studies [12, 13, 27, 49]: as corrosion progresses, the values of the mechanical properties decrease, while the yield plateau gradually disappears, leading to brittle failure at higher corrosion levels; the decrease in values of yield strength and tensile strength is much smaller than the values of strain at maximum load.

The yield strength reduction of the corroded reinforcement in relation to the mean value of the uncorroded reinforcement is in the range of 5.6% to 9.5% for the corrosion level I (mean value 7.6%), 8.3% to 13.7% for corrosion level II (mean value 10.8%) and 11.7% to 14.8% for the corrosion level III (mean value 13.2%). These measured values are in relation to those from studies [12, 31], which are based on various research results in which the values of the yield loss are between 1.2 and 2 times the mass loss.

The degradation of the tensile strength is lower than the degradation of the yield strength. This is consistent with most of the previous research results shown in [12, 17]. The degradation values of the tensile strength are between 4.53 % and 8.48 % for the corrosion level I (mean value 5.7 %), between 6.56 % and 8.77 % for the corrosion level II (mean value 8.04 %) and between 7.89 % and 12.87 % for the corrosion level III (mean value 10.82 %). The measured values are also in relation to the values in Imperatore [12] and Fernandez and Berrocal [31], where the yield strength loss is defined as 1.1 to 1.8 times the mass loss. The ratio of tensile strength to yield strength shows little variation in the range of 1.15 to 1.25 for corroded and uncorroded bar specimens what corresponds to the ratios shown in [38], where values range between 1.08 and 1.22.

A large variation in the reduction of the strain at maximum load is observed, which was expected according to the results of previous studies [17]. The values of the reductions are as follows: -0.14% to 39.54% for the corrosion level I (mean value 19.91%), 12.41% to 24.39% for the corrosion level II (mean value 18.18%) and 0.29% to 45.74% for the corrosion level III (with a mean value of 29%). As it can be seen the values of the strain at maximum load degradation are up to 5 times greater (mean value 2.6) than degradation of strengths what is in range of the results shown in Imperatore et al. [17].

The reduction in the modulus of elasticity shows a certain scatter, which fortunately is less than the scatter observed in the reduction of the strain at maximum load. The reduction values are between 1.34 % and 20.19 %. There is no obvious trend in terms of corrosion progression. The decrease in modulus of elasticity is not a common parameter investigated in previous studies on corrosion-damaged reinforcement. Only François et al. [30] show the modulus of elasticity as a function of the diameter loss (where a small increase in modulus of elasticity is observed as corrosion progresses), but these values cannot be compared with the values obtained in this study as the values in François et al. [30] were defined from stress-strain diagrams related to corroded rebar cross-section.

4. Degradation Models of Corroded Reinforcement

Models for evaluation of mechanical properties of corroded hot-rolled reinforcement are established in relation to the relative corrosion depths. The following mechanical properties of corroded and uncorroded bars were analyzed: yield strength, tensile strength, ratio of tensile strength to yield strength, modulus of elasticity and strain at maximum load.

Corrosion damage to reinforcing bars, expressed as relative corrosion depths, was assessed in two ways:

(i) By evaluating the mean corrosion depths $P_{i,corr}$ based on the corrosion rate measurement using the non-destructive electrochemical galvanostatic pulse technique;

(ii) By measuring the pit depths P_{pit} on corroded bars extracted from the beam specimens (destructive technique).

The relative corrosion depths are determined with respect to the initial diameter ϕ_0 of the reinforcing bars (P_{pit}/ϕ_0 and $P_{i,corr}/\phi_0$), while the mechanical properties of the corroded bars were normalized to the corresponding values of the uncorroded reinforcing bars. Only in Hingorani et al. [55] the remaining mechanical properties of the corroded reinforcement are related in the same way as in this study – to the relative corrosion depth based on the pit measurement (P_{pit}/ϕ_0) rather than to the residual cross-section or the mass of the rebar. To the author´s knowledge, there is no previous study that relates the remaining mechanical properties to the relative corrosion depths based on the corrosion rate measurement ($P_{i,corr}/\phi_0$). The creation of models based on destructive and non-destructive techniques is therefore aimed at the comparative evaluation of two different models based on the same experimental research.

In order to establish models for evaluation of mechanical properties of corroded reinforcement, the relationships between the experimentally determined relative corrosion depths (P_{pit}/ϕ_0 and $P_{i,corr}/\phi_0$) and the mechanical properties of the corroded reinforcement are shown in Figures 12 to 21. The degradation models in Figures 12 to 21 are represented by regression curves.

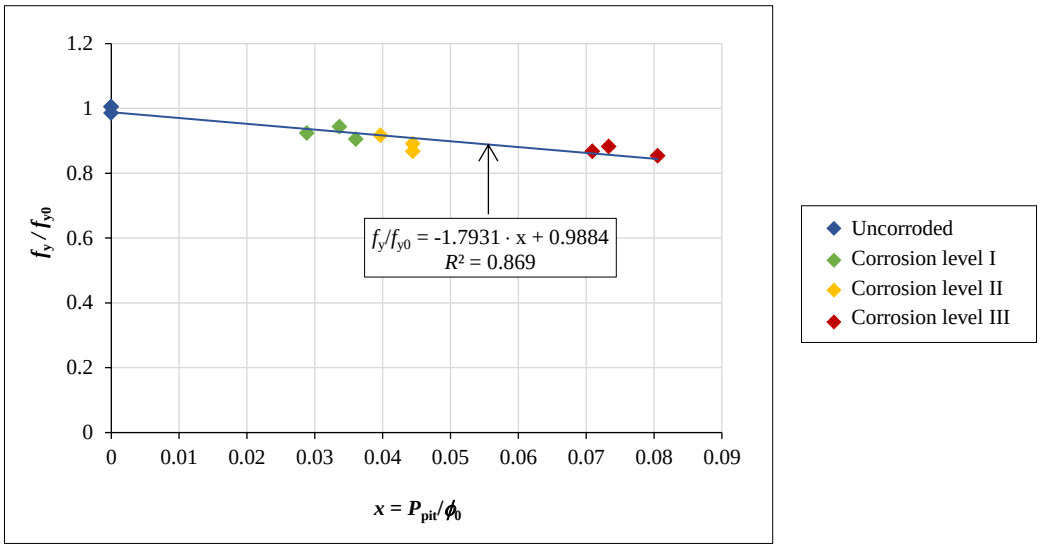

Figure 12. Ratio of the yield strength of corroded bars f_y to the mean yield strength of uncorroded bars f_{y0} = 589 MPa vs. the relative pit depth P_{pit}/ϕ_0

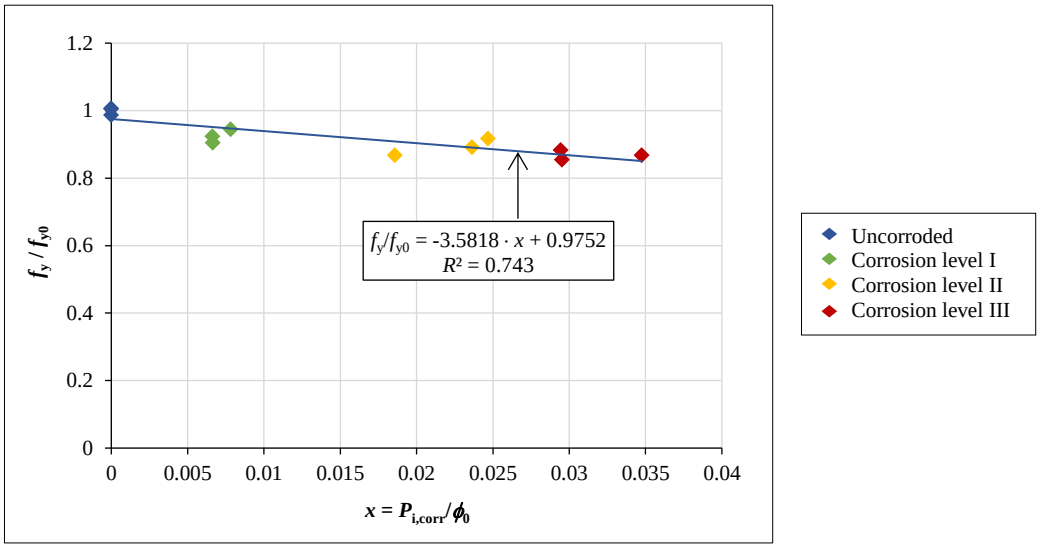

Figure 13. Ratio of the yield strength of corroded bars f_y to the mean yield strength of uncorroded bars f_{y0} = 589 MPa vs. the relative mean corrosion depth $P_{i,corr}/\phi_0$

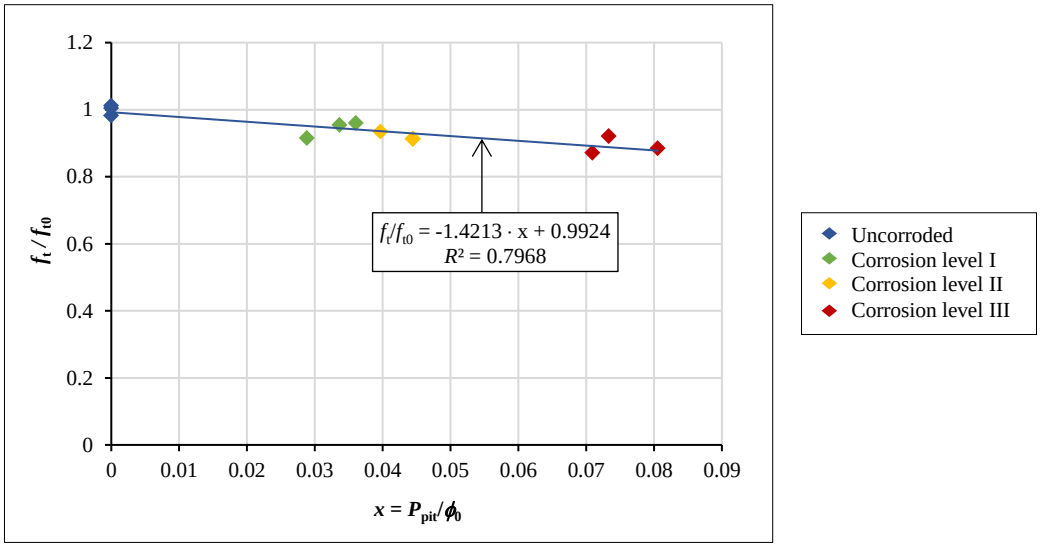

Figure 14. Ratio of the tensile strength of corroded bars f_t to the mean tensile strength of uncorroded bars f_{t0} = 684 MPa vs. the relative pit depth P_{pit}/ϕ_0

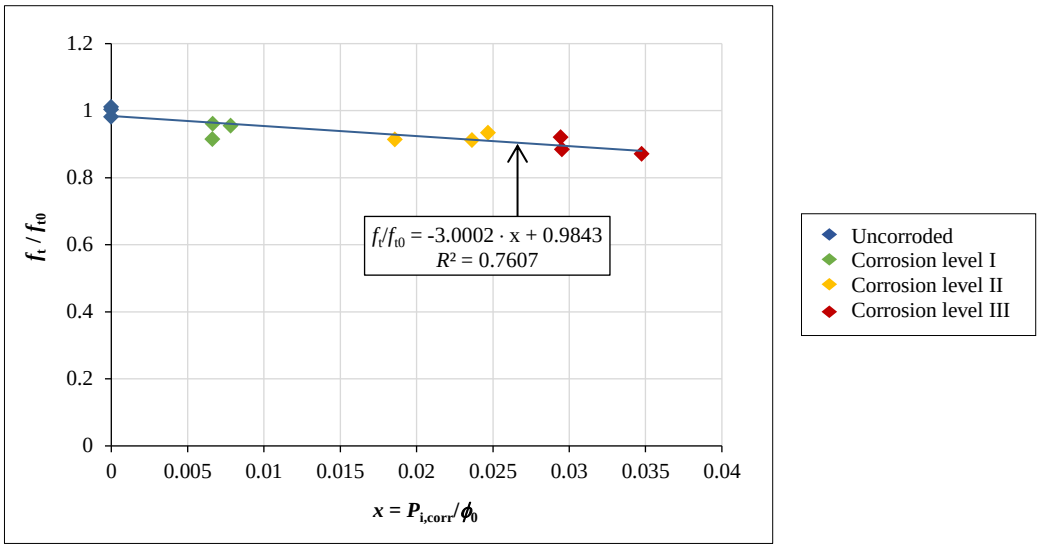

Figure 15. Ratio of the tensile strength of corroded bars f_t to the mean tensile strength of uncorroded bars f_{t0} = 684 MPa vs. the relative mean corrosion depth $P_{i,corr}/\phi_0$

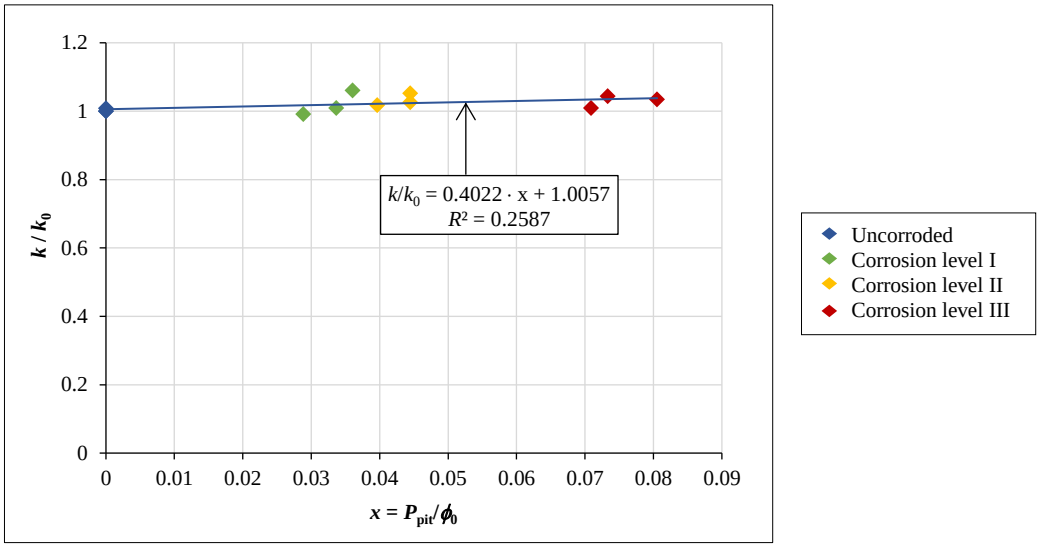

Figure 16. Ratio of the tensile strength to yield strength of corroded bars $k = f_t/f_y$ to the mean strength ratio of uncorroded bars k_0 = 1.16 vs. the relative pit depth P_{pit}/ϕ_0

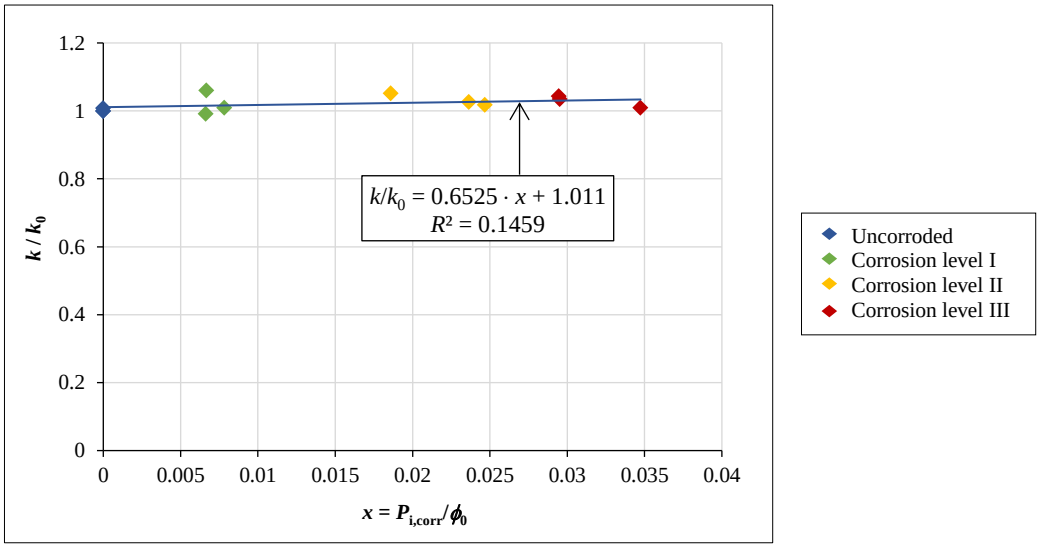

Figure 17. Ratio of the tensile strength to yield strength of corroded bars $k = f_t/f_y$ to the mean strength ratio of uncorroded bars k_0 = 1.16 vs. the relative mean corrosion depth $P_{i,corr}/\phi_0$

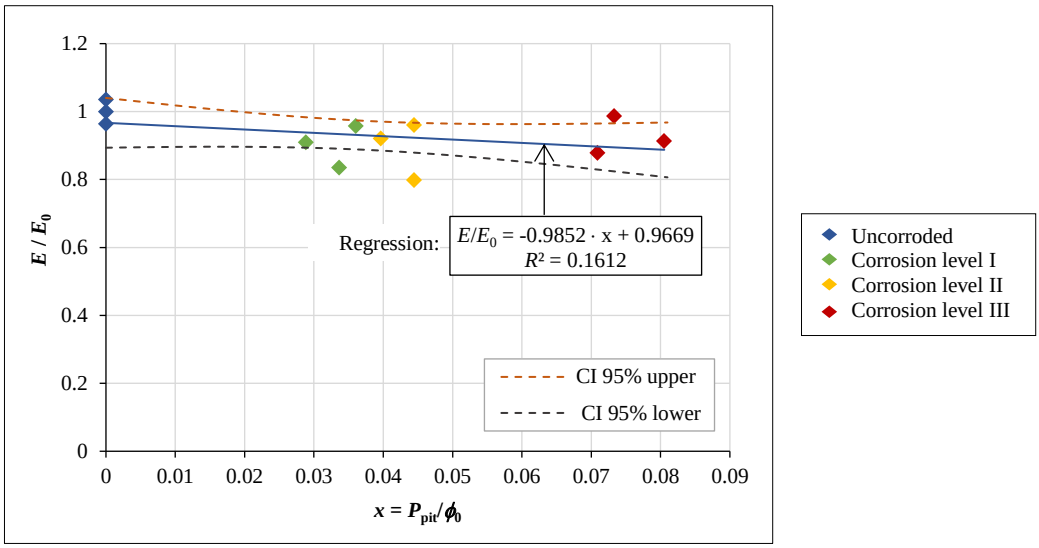

Figure 18. Ratio of the modulus of elasticity of corroded bars E to the mean modulus of uncorroded bars E_0 = 191807 MPa vs. the relative pit depth P_{pit}/ϕ_0

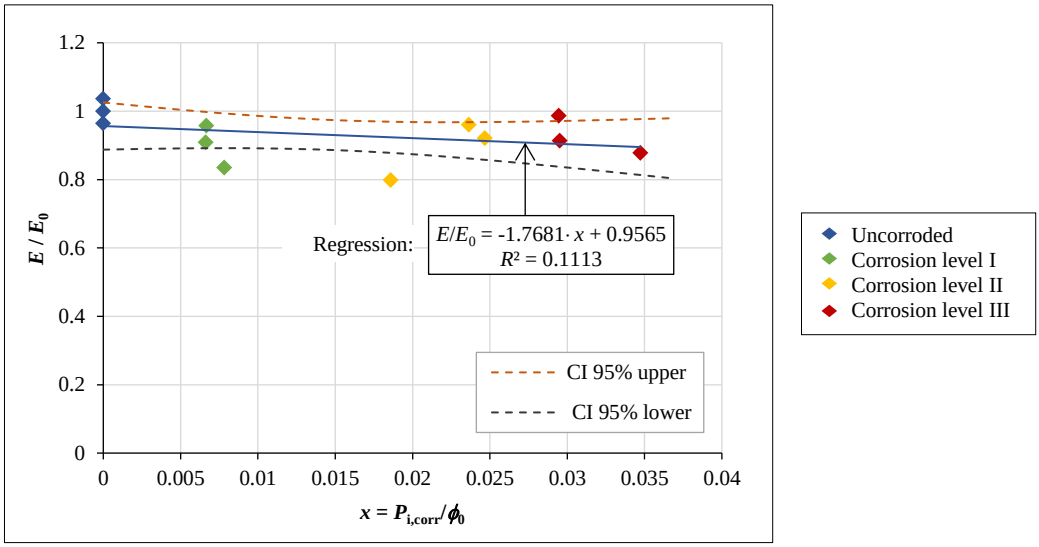

Figure 19. Ratio of the modulus of elasticity of corroded bars E to the mean modulus of uncorroded bars E0 = 191807 MPa vs. the relative mean corrosion depth Pi,corr/ϕ0

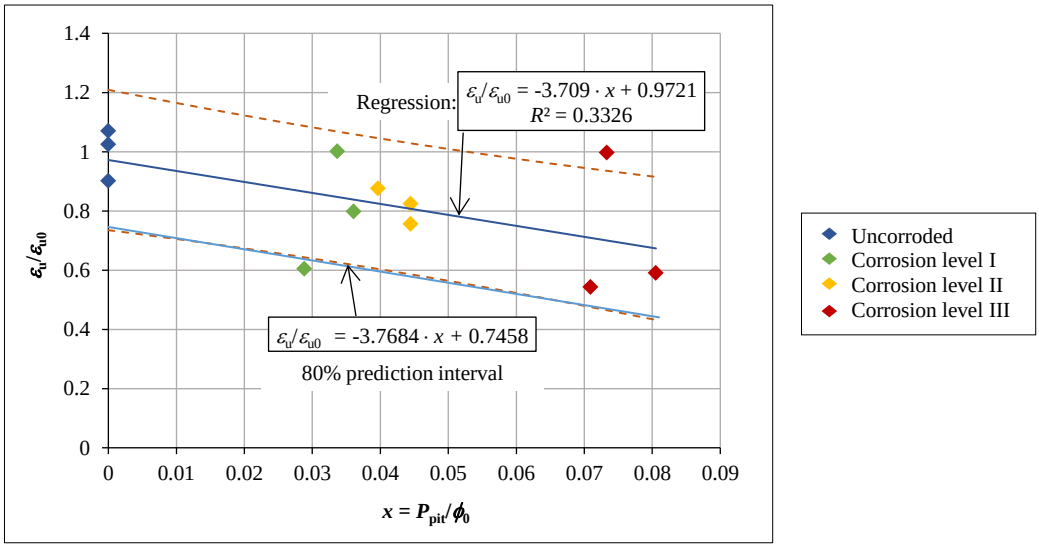

Figure 20. Ratio of the strain at maximum load of corroded bars ε_u to the mean strain at maximum load of uncorroded bars ε_{u0} = 6.93 % vs. the relative pit depth P_{pit}/ϕ_0

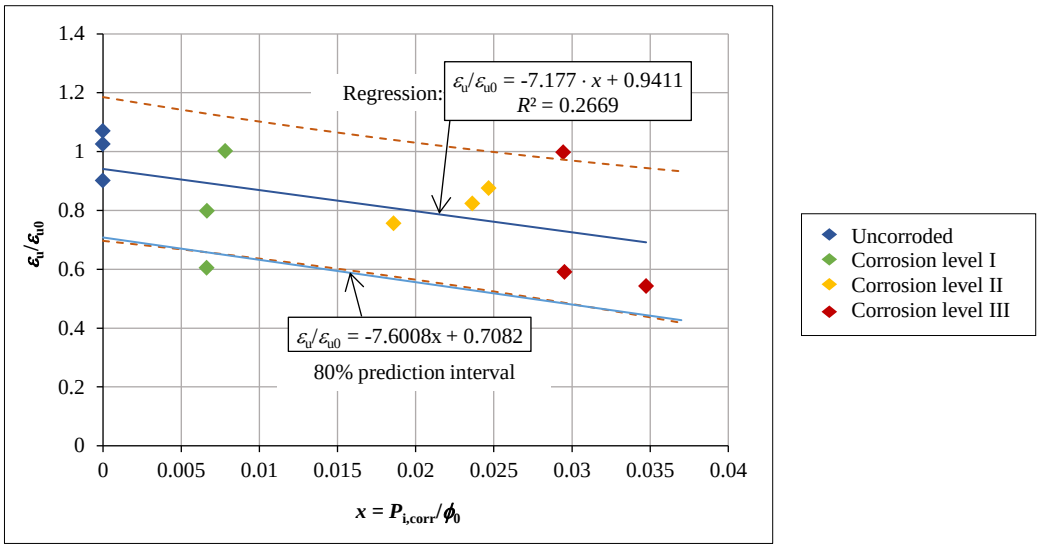

Figure 21. Ratio of the strain at maximum load of corroded bars ε_u to the mean strain at maximum load of uncorroded bars ε_{u0} = 6.93 % vs. the relative mean corrosion depth $P_{i,corr}/\phi_0$

A strong correlation between the relative corrosion depths (P_{pit}/ϕ_0 and $P_{i,corr}/\phi_0$) and the yield strength of the bars are established, as it can be seen in Figures 12 and 13.

The degradation models for yield strength are linear and similar. It can also be observed that the yield strength values in Figure 13 are mostly below the regression line for corrosion level I, whereas this is not the case in Figure 12. This can be explained by the large pitting factor, which was determined for small corrosion depths $P_{i,corr}$ and which decreases significantly as corrosion progresses, as shown in Figure 7 and in Yu et al. [7] and Cairns et al. [13].

Considering study by Hingorani et al. [55] [55], the linear relationship between the relative pith depth P_{pit}/ϕ_0 and the yield strength was not expected. Numerical studies on bars with pits showed that the relationship between the increase in the relative pit depth and the reduction in the yield strength is not linear – as the pit depth increases the gradient of the yield strength reduction increases. In general, the higher degradation rate is observed in this study than in Hingorani et al. [55]: for example, tensile strength degradation from Figure 12 at P_{pit}/ϕ_0 = 0.08 is 0.845 while in Hingorani et al. [55] it reaches the value of 0.96. However, it should also be noted that the pit width as well as their shape was not varied in Hingorani et al. [55] (pits were modelled as ellipsoids).

The observed linear relationship between the relative corrosion depths (P_{pit}/ϕ_0 and $P_{i,corr}/\phi_0$) and the yield strength in Figures 12 and 13 can be explained by the reinforcement corrosion progression process:

- Initially, the corrosion is strongly localized with a relatively large pit depth compared to the average corrosion depth at the measuring range of the corrosion rate sensor (large pitting factor in Figure 7). This leads to a greater reduction in the bar strengths compared to that which can be estimated on the basis of the mean corrosion depth.
- Thereafter, the pit depth increases simultaneously with their width, resulting in a smaller strength difference in relation to the measured relative pit depths P_{pit}/ϕ_0 and to the relative mean corrosion depths, based on the corrosion rate measurement, $P_{i,corr}/\phi_0$.
- The decrease in the pitting factor α with the increase in the relative corrosion depth $P_{i,corr}/\phi_0$, as shown in Figure 7 and illustrated in the study by Yu et al. [7], shows that the corrosion is less and less localized as the reinforcement corrosion progresses.

As a conclusion, it may be observed that the accuracy of the yield strength estimation of corroded bars based on corrosion monitoring is increasing with the progress of the corrosion process.

Figures 14 and 15 show a strong correlation between the relative corrosion depths (P_{pit}/ϕ_0 and $P_{i,corr}/\phi_0$) and the tensile strength of the bars. The models for tensile strength degradation shown in Figures 14 and 15 are linear and similar. There is no relevant literature that could be compared with the results based on relative corrosion depth, but slight decrease of tensile strength with corrosion progress expressed as mass loss or cross-sectional loss is presented by most of the researchers [12, 17]. For example, if the mass loss of corroded reinforcement is 7.5% (what corresponds with the corrosion level III) the tensile strength ratio is between 86.5% and 92% [12].

Figures 16 and 17 show that the impact of reinforcement corrosion on the ratio of tensile strength to yield strength $k = f_t/f_y$ is negligible for corrosion levels reached in the experimental research (P_{pit}/ϕ_0 up to 0.081; $P_{i,corr}/\phi_0$ up to 0.035). Similar trends can be seen from the results presented in Chen et al. [49], where the ratio of tensile strength to yield strength of corroded reinforcement with regard to strength ratios for uncorroded reinforcement is between 1 and 1.02 up to 10% of the cross-sectional loss. According to Hingorani et al. [55] the ratio of tensile strength to yield strength of

corroded reinforcement in relation to the ratios obtained for uncorroded reinforcement is almost constant up to $P_{pit}/\phi_0 =$ 0.2 and ranges roughly between 1 and 0.95.

Figures 18 and 19 show the relationship between the ratio of the modulus of elasticity of the corroded bars and the corresponding mean value of the uncorroded bars E/E_0 and the relative corrosion depths ($P_{i,corr}/\phi_0$ and P_{pit}/ϕ_0). A weak correlation is found between the ratio of the modulus of elasticity E/E_0 and the relative corrosion depths. The degradation models for the modulus of elasticity are linear and similar. Figures 18 and 19 also contain the lower and upper limits of the 95 % confidence interval (CI) for the mean values. The studies on changes in modulus of elasticity are rare as explained before: no relevant study to make the comparison is available.

Figures 20 and 21 show the relationship between the ratio of the strain at maximum load of corroded bars and the corresponding mean value for uncorroded bars $\varepsilon_u/\varepsilon_{u0}$ and the relative corrosion depths ($P_{i,corr}/\phi_0$ and P_{pit}/ϕ_0). It was established that the correlation between the ratio of strains $\varepsilon_u/\varepsilon_{u0}$ and the relative corrosion depths ($P_{i,corr}/\phi_0$ and P_{pit}/ϕ_0) is weak due to the great scatter of the experimental results. A greater scatter in the test results for ultimate strain than for yield or tensile strength can also be observed in a large number of test data [17]. A smaller scatter of the strain values ε_u would result if longer gauge lengths were used, as shown in Chen et al. [49].

A similar decrease in strain is observed in Chen et al. [49] and Hingorani et al. [55] as well. The equations for the regression lines and the functions of the lower values of the 80% prediction intervals are also shown in Figures 20 and 21. The prediction interval was selected in accordance with the requirements of EN 10080 [64]: the characteristic value of the strain ε_u is the value for which a maximum of 10% of the test results can be expected to be less than or equal to this value (10% fractile). According to Hingorani et al. [55], the relevant values for the reduction in strain at maximum load are 0.82 and 0.7 for P_{pit}/ϕ_0=0.04, or 0.6 and 0.53 for P_{pit}/ϕ_0=0.08, depending on the ellipsoid shape. These values lie within the regression and 80% prediction interval shown in Figure 20.

The degradation models of mechanical properties of corroded hot rolled steel bars expressed as regression lines in Figures 12 to 21 are similar for each mechanical property, regardless of whether the relative corrosion depth is determined by evaluating the mean corrosion depth $P_{i,corr}$ using the GPT monitoring or by measuring the pit depth $P_{pit.}$

The difference between the values of mechanical properties reduction of corroded reinforcement determined using models based on relative mean corrosion depth $P_{i,corr}/\phi_0$ and relative pit depth P_{pit}/ϕ_0 are as follows:

- up to 1% in case of yield strength, tensile strength and modulus of elasticity,
- up to 3% in case of strain at maximum load.

According to Hingorani et al. [55] if the mechanical properties of the reinforcement are determined as a function of the relative pit depth P_{pit}/ϕ_0, the diameter of the bars (scale effect) has no influence on the mechanical properties of the reinforcement. Same conclusion can be applied for the mechanical properties of the reinforcement determined as a function of the relative mean corrosion depth $P_{i,corr}/\phi_0$. This conclusion is based on the strong correlation between experimentally determined relative mean corrosion depth $P_{i,corr}/\phi_0$ and the pitting factor α, as well as on similar degradation models for each mechanical properties regardless of how the relative corrosion depth was determined.

5. Conclusions

Appropriate inspection, monitoring, and maintenance of buildings and infrastructures reduce life cycle costs and support sustainability. Reliable models for assessing the load-bearing capacity, serviceability, and ductility of RC structures exposed to reinforcement corrosion in a chloride-containing environment can serve as a decision-making basis for maintenance and repair management with the aim of reducing life cycle costs.

Existing methods for assessing the mechanical properties of corroded reinforcement are based on measurements and observation of corrosion damage on bars (pits, cross-sectional reduction, shape, and distribution of corrosion damage) in existing RC structures and relating this damage to the remaining mechanical properties of the corroded reinforcement. To carry them out, the concrete cover around the reinforcement must be removed, or the reinforcement bars have to be extracted from the structure, which is a destructive procedure that can only be carried out to a limited extent on an operational building. Among the existing models, there are a few degradation models of corroded reinforcement performed under environmental conditions (in real time or accelerated) on loaded specimens (to induce cracks that occur under service load).

The advantages of assessing the mechanical properties of corroded reinforcement based on the results of structural health monitoring using the galvanostatic pulse technique (corrosion monitoring) shown in this paper are as follows:

- GPT is a fast, cost-effective, non-destructive method that can be applied relatively easily to existing in-service structures.
- It is not necessary to know the remaining cross-section of the corroded bar in order to determine its mechanical properties because all the mechanical properties of the corroded reinforcement, as well as the relative corrosion depths, are determined with respect to the initial bar cross-section.

- There is no scale effect when the mechanical properties are determined as a function of the relative corrosion depth.

The degradation models for the yield strength, tensile strength, tensile strength to yield strength ratio, modulus of elasticity, and strain at maximum load proposed in this paper are based on the results of an extensive long-term experimental study on RC beams subjected to simultaneous loading and accelerated chloride corrosion in an environmental chamber.

The degradation models of the mechanical properties as functions of the relative corrosion depths determined by non-destructive monitoring ($P_{i,corr}/\phi_0$) are similar to those based on destructive methods (P_{pit}/ϕ_0) for each mechanical property considered in this study. The relative corrosion depths and the yield strength or tensile strength of the corroding reinforcement show a strong correlation. Therefore, the yield strength and tensile strength of the corroded reinforcement can be reliably evaluated both from the pit measurement and from the periodic measurement of the corrosion rate using the GPT in a RC structure (corrosion monitoring). A negligible influence of reinforcement corrosion on the ratio of tensile strength to yield strength was measured.

Mechanical properties related to ductility (strain at maximum load and ratio of tensile strength to yield strength) are weakly correlated to the relative mean corrosion depths determined from corrosion rate measurements and to the relative pits depth. The strain of the corroded reinforcement at maximum load shows a significant scatter in the measurement results for each of the three corrosion levels. Therefore, when evaluating the strain of the corroded reinforcement at maximum load, we suggest selecting the lower limit of the 80% prediction interval.

A weak correlation is also found between the ratio of the modulus of elasticity and the relative corrosion depths. However, for the evaluation of the remaining bending stiffness of beams with corroded reinforcement and their deflections under load, these deviations from the regression line are not significant, since the deflection of the beam is determined as the double integral of the curvature over the entire length of the beam. It is therefore sufficient to estimate the mean modulus of elasticity of the corroded reinforcement.

In order to increase the reliability of the proposed method, it is necessary to calibrate the models for evaluation of the mechanical properties of corroded reinforcement on the basis of a larger number of studies in which the corrosion rate is monitored and the mechanical properties of corroded reinforcing bars extracted from RC members are determined. Such studies should be carried out under controlled laboratory conditions and as part of the corrosion monitoring of existing RC structures.

6. Declarations

6.1. Author Contributions

Conceptualization, D.G. and I.S.G.; methodology, D.G.; validation, D.G. and I.S.G.; formal analysis, D.G.; investigation, D.G.; resources, D.G. and I.S.G.; data curation, D.G.; writing—original draft preparation, D.G. and I.S.G.; writing—review and editing, I.S.G. and P.S.; visualization, D.G. and P.S.; project administration, I.S.G.; funding acquisition, I.S.G. All authors have read and agreed to the published version of the manuscript.

6.2. Data Availability Statement

The data presented in this study are available on request from the corresponding author.

6.3. Funding and Acknowledgments

Financial support from the University of Rijeka, through Grant No. uniri-tehnic-18-127, is gratefully acknowledged.

6.4. Conflicts of Interest

The authors declare no conflict of interest.

7. References

[1] Gomasa, R., Talakokula, V., Kalyana Rama Jyosyula, S., & Bansal, T. (2023). A review on health monitoring of concrete structures using embedded piezoelectric sensor. Construction and Building Materials, 405, 133179. doi:10.1016/j.conbuildmat.2023.133179.

[2] Kim, S., Jeong, Y., Kwon, M., & Kim, J. (2024). Combined deterioration effects of freeze–thaw and corrosion on the cyclic flexural behavior of RC beams. Journal of Building Engineering, 84, 108564. doi:10.1016/j.jobe.2024.108564.

[3] Shevtsov, D., Cao, N. L., Nguyen, V. C., Nong, Q. Q., Le, H. Q., Nguyen, D. A., Zartsyn, I., & Kozaderov, O. (2022). Progress in Sensors for Monitoring Reinforcement Corrosion in Reinforced Concrete Structures—A Review. Sensors, 22(9), 3421. doi:10.3390/s22093421.

[4] Ebell, G., Mayer, T. F., Harnisch, J., & Dauberschmidt, C. (2024). Corrosion monitoring of reinforced concrete structures: The DGZfP specification B12 Collaboration. Materials and Corrosion, 75(2), 188–196. doi:10.1002/maco.202313934.

[5] Bras, A., van der Bergh, J. M., Mohammed, H., & Nakouti, I. (2021). Design service life of RC structures with self-healing behaviour to increase infrastructure carbon savings. Materials, 14(12), 3154. doi:10.3390/ma14123154.

[6] Verma, S. K., Bhadauria, S. S., & Akhtar, S. (2016). In-situ condition monitoring of reinforced concrete structures. Frontiers of Structural and Civil Engineering, 10(4), 420–437. doi:10.1007/s11709-016-0336-z.

[7] Yu, L., François, R., Dang, V. H., L'Hostis, V., & Gagné, R. (2015). Distribution of corrosion and pitting factor of steel in corroded RC beams. Construction and Building Materials, 95, 384–392. doi:10.1016/j.conbuildmat.2015.07.119.

[8] Trejo, D., Halmen, C., & Reinschmidt, K. (2009). Corrosion performance tests for reinforcing steel in concrete: technical report. No. FHWA/TX-09/0-4825-1, Texas Transportation Institute, Bryan, United States.

[9] Bahleda, F., Prokop, J., Koteš, P., & Wdowiak-Postulak, A. (2023). Mechanical Properties of Corroded Reinforcement. Buildings, 13(4), 855. doi:10.3390/buildings13040855.

[10] Li, C. Q., Zheng, J. J., & Shao, L. (2003). New Solution for Prediction of Chloride Ingress in Reinforced Concrete Flexural Members. ACI Materials Journal, 100(4), 319–325. doi:10.14359/12670.

[11] Broomfield, J.P. (2007). Corrosion of Steel in Concrete: Understanding, Investigation and Repair (2nd Ed.). CRC Press, Boca Raton, United States.

[12] Imperatore, S. (2022). Mechanical Properties Decay of Corroded Reinforcement in Concrete—An Overview. Corrosion and Materials Degradation, 3(2), 210–220. doi:10.3390/cmd3020012.

[13] Cairns, J., Plizzari, G. A., Du, Y., Law, D. W., & Franzoni, C. (2005). Mechanical properties of corrosion-damaged reinforcement. ACI Materials Journal, 102(4), 256–264. doi:10.14359/14619.

[14] Imperatore, S., & Rinaldi, Z. (2008). Mechanical behaviour of corroded rebars and influence on the structural response of R/C elements. Concrete Repair, Rehabilitation and Retrofitting II (ICCRRR-2), 24–26 November 2008, Cape Town, South Africa.

[15] Rinaldi, Z., Imperatore, S., & Valente, C. (2010). Experimental evaluation of the flexural behavior of corroded P/C beams. Construction and Building Materials, 24(11), 2267–2278. doi:10.1016/j.conbuildmat.2010.04.029.

[16] Apostolopoulos, A., & Matikas, T. E. (2016). Corrosion of bare and embedded in concrete steel bar-impact on mechanical behavior. International Journal of Structural Integrity, 7(2), 240–259. doi:10.1108/IJSI-09-2014-0047.

[17] Imperatore, S., Rinaldi, Z., & Drago, C. (2017). Degradation relationships for the mechanical properties of corroded steel rebars. Construction and Building Materials, 148, 219–230. doi:10.1016/j.conbuildmat.2017.04.209.

[18] Zhu, W. (2014). Effect of corrosion on the mechanical properties of the corroded reinforcement and the residual structural performance of the corroded beams. Ph.D. Thesis, Université de Toulouse, Toulouse, France.

[19] Yuan, Y., Ji, Y., & Shah, S. P. (2007). Comparison of two accelerated corrosion techniques for concrete structures. ACI Structural Journal, 104(3), 344–347. doi:10.14359/18624.

[20] Grandić, D., & Bjegović, D. (2011). Reinforcement Corrosion Rate in Cracked Areas of RC-Members Subjected to Sustained Load. Modelling of Corroding Concrete Structures: Proceedings of the Joint fib-RILEM Workshop held in Madrid, Spain, 22–23 November 2010, 65–83. doi:10.1007/978-94-007-0677-4_4.

[21] Grandić, D., Bjegović, D., & Serdar, M. (2009). Chloride threshold for different levels of reinforcement corrosion propagation. In 2nd International RILEM Workshop. Haifa, Israel, 7-9 September 2009, 416-422.

[22] Šćulac, P., Davor, G., & Štimac Grandić, I. (2020). Degradation of tension stiffening due to corrosion-an experimental study on cracked specimens. In 2nd International Conference on Construction Materials for a Sustainable Future COMS_2020/21, 287-294.

[23] Caprili, S., & Salvatore, W. (2018). Mechanical performance of steel reinforcing bars in uncorroded and corroded conditions. Data in Brief, 18, 1677–1695. doi:10.1016/j.dib.2018.04.072.

[24] Hong, S., Zheng, F., Shi, G., Li, J., Luo, X., Xing, F., Tang, L., & Dong, B. (2020). Determination of impressed current efficiency during accelerated corrosion of reinforcement. Cement and Concrete Composites, 108, 103536. doi:10.1016/j.cemconcomp.2020.103536.

[25] El Maaddawy, T., Soudki, K., & Topper, T. (2005). Long-term performance of corrosion-damaged reinforced concrete beams. ACI Structural Journal, 102(5), 649–656. doi:10.14359/14660.

[26] Poupard, O., L'Hostis, V., Bouteiller, V., Capra, B., Catinaud, S., Francois, D., Garciaz, J.-L., Laurens, S., Luping, T., Olivier, G., & Tache, G. (2007). Corrosion diagnosis of reinforced concrete beams after 40 years exposure in marine environment by non-destructive tools. Revue Européenne de Génie Civil, 11(1–2), 35–54. doi:10.1080/17747120.2007.9692921.

[27] Zhu, W., François, R., Poon, C. S., & Dai, J. G. (2017). Influences of corrosion degree and corrosion morphology on the ductility of steel reinforcement. Construction and Building Materials, 148, 297–306. doi:10.1016/j.conbuildmat.2017.05.079.

[28] Zhu, W., & Francois, R. (2013). Effect of corrosion pattern on the ductility of tensile reinforcement extracted from a 26-year-old corroded beam. Advances in Concrete Construction, 1(2), 121–136. doi:10.12989/acc2013.01.2.121.

[29] Zhu, W., & François, R. (2014). Experimental investigation of the relationships between residual cross-section shapes and the ductility of corroded bars. Construction and Building Materials, 69, 335–345. doi:10.1016/j.conbuildmat.2014.07.059.

[30] François, R., Khan, I., & Dang, V. H. (2012). Impact of corrosion on mechanical properties of steel embedded in 27-year-old corroded reinforced concrete beams. Materials and Structures, 46(6), 899–910. doi:10.1617/s11527-012-9941-z.

[31] Fernandez, I., & Berrocal, C. G. (2019). Mechanical Properties of 30 Year-Old Naturally Corroded Steel Reinforcing Bars. International Journal of Concrete Structures and Materials, 13(1), 9. doi:10.1186/s40069-018-0308-x.

[32] Apostolopoulos, C. A., Demis, S., & Papadakis, V. G. (2013). Chloride-induced corrosion of steel reinforcement - Mechanical performance and pit depth analysis. Construction and Building Materials, 38, 139–146. doi:10.1016/j.conbuildmat.2012.07.087.

[33] Alzabeebee, S., Al‐ Hamd, R. K. S., Nassr, A., Kareem, M., & Keawsawasvong, S. (2023). Multiscale soft computing-based model of shear strength of steel fibre-reinforced concrete beams. Innovative Infrastructure Solutions, 8(1), 63. doi:10.1007/s41062-022-01028-y.

[34] Morinaga, S. (1988). Prediction of service lives of reinforced concrete buildings based on the rate of corrosion. Shimizu Institute of Technology, Tokyo, Japan.

[35] Poursaee, A., & Hansson, C. M. (2009). Potential pitfalls in assessing chloride-induced corrosion of steel in concrete. Cement and Concrete Research, 39(5), 391–400. doi:10.1016/j.cemconres.2009.01.015.

[36] Robuschi, S., Ivanov, O. L., Geiker, M., Fernandez, I., & Lundgren, K. (2022). Impact of cracks on distribution of chloride-induced reinforcement corrosion. Materials and Structures, 56(1). doi:10.1617/s11527-022-02085-6.

[37] Rodríguez, J., Ortega, L. M., Aragoncillo, J., Izquieredo, D., & Andrade, C. (2000). Structural assessment methodology for residual life calculation of concrete structures affected by reinforcement corrosion. International RILEM Workshop on Life Prediction and Aging Management of Concrete Structures, RILEM Publications SARL, 16-17 October, 2000, Cannes, France.

[38] Rodríguez, J., Aragoncillo, J., Andrade, C., & Izquierdo, D. (2002). Contecvet. A validated User's Manual for assessing the residual service life of concrete structures. Manual for assessing corrosion-affected concrete structures. EC Innovation Programme IN30902I, GEOCISA, Madrid, Spain.

[39] Val, D. V., & Melchers, R. E. (1997). Reliability of Deteriorating RC Slab Bridges. Journal of Structural Engineering, 123(12), 1638–1644. doi:10.1061/(asce)0733-9445(1997)123:12(1638).

[40] Stewart, M. G., & Al-Harthy, A. (2008). Pitting corrosion and structural reliability of corroding RC structures: Experimental data and probabilistic analysis. Reliability Engineering & System Safety, 93(3), 373–382. doi:10.1016/j.ress.2006.12.013.

[41] Lay, S. & Schießl, P. (2003) Lifecon Deliverable D 3.2 - Service Life Models. Technische Universität München, München, Germany.

[42] González, J. A., Andrade, C., Alonso, C., & Feliu, S. (1995). Comparison of rates of general corrosion and maximum pitting penetration on concrete embedded steel reinforcement. Cement and Concrete Research, 25(2), 257–264. doi:10.1016/0008-8846(95)00006-2.

[43] Mangat, P. S., & Elgarf, M. S. (1999). Flexural strength of concrete beams with corroding reinforcement. ACI Structural Journal, 96(1), 149–158. doi:10.14359/606.

[44] Frølund, T., Klinghoffer, O., & Poulsen, E. (2000). Rebar corrosion rate measurements for service life estimates. ACI Fall Convention, 17-18 October, Toronto, Canada.

[45] Grandić, D., & Štimac Grandić, I. (2021). Pitting factor in use of galvanostatic pulse method for measuring the corrosion rate of reinforcement in concrete. Machines. Technologies. Materials. 15(7), 259-263.

[46] Palsson, R., & Mirza, M. S. (2002). Mechanical response of corroded steel reinforcement of abandoned concrete bridge. ACI Structural Journal, 99(2), 157–162. doi:10.14359/11538.

[47] Tang, F., Lin, Z., Chen, G., & Yi, W. (2014). Three-dimensional corrosion pit measurement and statistical mechanical degradation analysis of deformed steel bars subjected to accelerated corrosion. Construction and Building Materials, 70, 104–117. doi:10.1016/j.conbuildmat.2014.08.001.

[48] Fernandez, I., Lundgren, K., & Zandi, K. (2018). Evaluation of corrosion level of naturally corroded bars using different cleaning methods, computed tomography, and 3D optical scanning. Materials and Structures, 51(3), 1-13. doi:10.1617/s11527-018-1206-z.

[49] Chen, E., Berrocal, C. G., Fernandez, I., Löfgren, I., & Lundgren, K. (2020). Assessment of the mechanical behaviour of reinforcement bars with localised pitting corrosion by Digital Image Correlation. Engineering Structures, 219, 110936. doi:10.1016/j.engstruct.2020.110936.

[50] Wang, X. G., Zhang, W. P., Gu, X. L., & Dai, H. C. (2013). Determination of residual cross-sectional areas of corroded bars in reinforced concrete structures using easy-to-measure variables. Construction and Building Materials, 38, 846–853. doi:10.1016/j.conbuildmat.2012.09.060.

[51] Turnbull, A., Horner, D. A., & Connolly, B. J. (2009). Challenges in modelling the evolution of stress corrosion cracks from pits. Engineering Fracture Mechanics, 76(5), 633–640. doi:10.1016/j.engfracmech.2008.09.004.

[52] Du, Y. G., Clark, L. A., & Chan, A. H. C. (2005). Effect of corrosion on ductility of reinforcing bars. Magazine of Concrete Research, 57(7), 407–419. doi:10.1680/macr.2005.57.7.407.

[53] Ou, Y. C., Susanto, Y. T. T., & Roh, H. (2016). Tensile behavior of naturally and artificially corroded steel bars. Construction and Building Materials, 103, 93–104. doi:10.1016/j.conbuildmat.2015.10.075.

[54] Finozzi, I., Saetta, A., & Budelmann, H. (2018). Structural response of reinforcing bars affected by pitting corrosion: experimental evaluation. Construction and Building Materials, 192, 478–488. doi:10.1016/j.conbuildmat.2018.10.088.

[55] Hingorani, R., Pérez, F., Sánchez, J., Fullea, J., Andrade, C., & Tanner, P. (2013). Loss of ductility and strength of reinforcing steel due to pitting corrosion. Proceedings of the 8th International Conference on Fracture Mechanics of Concrete and Concrete Structures, FraMCoS 2013, 2009–2018.

[56] Grandić, D. (2008). Calculation procedures for evaluating remaining load bearing capacity and serviceability of corroded reinforced concrete structures. Ph.D. thesis. Faculty of Civil Engineering, University of Zagreb. Croatia. (in Croatian).

[57] ASTM C1202-19. (2022). Standard Test Method for Electrical Indication of Concrete's Ability to Resist Chloride Ion Penetration. ASTM International, Pennsylvania, United States. doi:10.1520/C1202-19.

[58] Ukrainczyk, V., & Bjegović, D. (1995). Materials testing in the insurance system of durability of concrete structures. Civil engineering yearbook, 209-286. (in Croatian)

[59] Li, C. Q. (2003). Initiation of chloride-induced reinforcement corrosion in concrete structural members - Prediction. ACI Structural Journal, 100(1), 126–127. doi:10.14359/10293.

[60] Li, C. Q. (2002). Initiation of chloride-induced reinforcement corrosion in concrete structural members - Prediction. ACI Structural Journal, 99(2), 133–141. doi:10.14359/11535.

[61] Nygaard, P. V., Geiker, M. R., & Elsener, B. (2009). Corrosion rate of steel in concrete: Evaluation of confinement techniques for on-site corrosion rate measurements. Materials and Structures, 42(8), 1059–1076. doi:10.1617/s11527-008-9443-1.

[62] Brite-Euram, I. I. I. (2002). Smart Structures. Contract No. BRPR-CT98-0751: Integrated Monitoring Systems for Durability Assessment of Concrete Structures, Project Report, September, 2002.

[63] EN10002-1. (2001). Metallic materials - Tensile testing – Part 1: Method of test at ambient temperature. European Committee for Standardization. Brussels, Belgium.

[64] EN 10080. (2005). Steel for the reinforcement of concrete – Weldable reinforcing steel – General. European Committee for Standardization. Brussels, Belgium.